Analytic and Numeric Tests of Fourier Deformation Model

Although the solutions of our Fourier deformation model have been checked using computer algebra, it is necessary to verify the accuracy of our computer code through comparison with known analytic solutions. Faulting behavior for our Fourier model is simulated by imbedding a prescribed fault in a 1-km spaced grid, performing a 2-D horizontal Fourier transform of the grid, multiplying by appropriate transfer functions, and inverse transforming to arrive at the final solution. The following tests and comparisons have been made:

i.) 2-D analytic tests
   a.) Homogeneous elastic half-space [*Weertman*, 1964]
   b.) Layered elastic half-space [*Rybicki*, 1971]
   c.) Non-surface observation planes [*Savage and Lisowski*, 1993]
   d.) Layered viscoelastic half-space [*Nur and Mavko*, 1977]

ii.) 2-D analytic Boussinesq tests
   a.) 2-D analytic point load solution [*Love*, 1944]
   b.) Half-space and a plate model comparisons with gravity
   c.) Analytic flexure solution [*Le Pichon et al*., 1973]
   d.) Trench flexure solution [*Turcotte and Schubert*, 2001, p. 127]

iii.) 3-D *Okada* [1985,1992] model comparison
   a.) Demonstration of single couple (deep slip) model
   b.) Demonstration of double couple (shallow slip) model

iv.) Demonstration of sign convention
   a.) Straight fault geometry
   b.) Diagonally-oriented fault geometry

v.) Comparison of elastic and viscoelastic San Andreas model

vi.) Example of time-dependence for viscoelastic San Andreas model

i) *2-D analytic tests*

Although the solutions of our Fourier model have been checked using computer algebra, it is necessary to verify the accuracy of our computer code through comparison with known analytic solutions. These include 2-D analytic examples for displacement of a fault plane in (1) a homogeneous elastic half-space (2) a layered elastic half-space and (3) a layered viscoelastic half-space. Faulting behavior for our Fourier model is simulated by imbedding an infinitely-long fault in the y-dimension in a 1-km spaced grid, performing a 2-D horizontal Fourier transform of the grid, multiplying by appropriate transfer functions, and inverse transforming to arrive at the final solution.

a) Homogeneous elastic half-space

As a basic test, we compare our Fourier-derived fault solution to 2-D analytic solutions for a homogeneous elastic half-space. The surface displacement due to a 2-D fault in a homogeneous elastic medium that is freely slipping between depths of d_1 and d_2 [*Weertman*, 1964] is:

$$V(x) = \frac{V_o}{\pi}\left[\tan^{-1}\left(\frac{x}{d_2}\right) - \tan^{-1}\left(\frac{x}{d_1}\right)\right]. \qquad (1)$$

This solution is often used to described the far-field behavior deep slip on a fault plane. For a fault that is locked between depths d_1 and d_2, the surface displacement due to a 2-D fault can be described by:

$$V(x) = \frac{-V_o}{\pi}\left[\tan^{-1}\left(\frac{d_2}{x}\right) - \tan^{-1}\left(\frac{d_1}{x}\right)\right]. \qquad (2)$$

This solution is often used to describe a minimum and maximum depth at which a fault plane is locked until an earthquake occurs. For both solutions, V_o = slip, d_1 = lower locking depth, d_2 = upper locking depth, and x = distance across fault-plane.

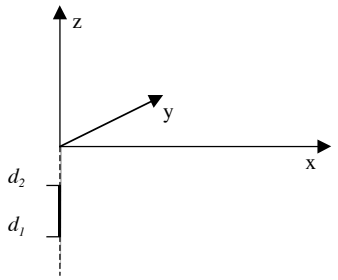

We can simulate both of these faulting behaviors for our Fourier-derived fault solution. In order to form a double-couple dislocation, we have constructed a screw dislocation by taking the derivative of the fault-source in the direction normal to the fault plane. This corresponds to multiplication in the Fourier domain. For this 2-D comparison, we imbed an infinitely-long fault in the y-dimension in a 1-km spaced grid, which is Fourier transformed, multiplied by the transfer functions described in earlier notes, and inverse Fourier transformed.

In order to test the deep slip case (Eq. 1), we assign an upper locking depth of 30 km (d_2) and extend the lower depth to infinity (d_1). For this test, we use the following parameters in both our Fourier model and for comparison with the analytic solution: d_1 = -100000 km, d_2 = -30 km, z = 0, and V_o = 1 mm. Figure 1 shows the comparison between a fault-perpendicular profile of our Fourier-derived grid results and that of the deep slip analytic solution (Eq. 1).

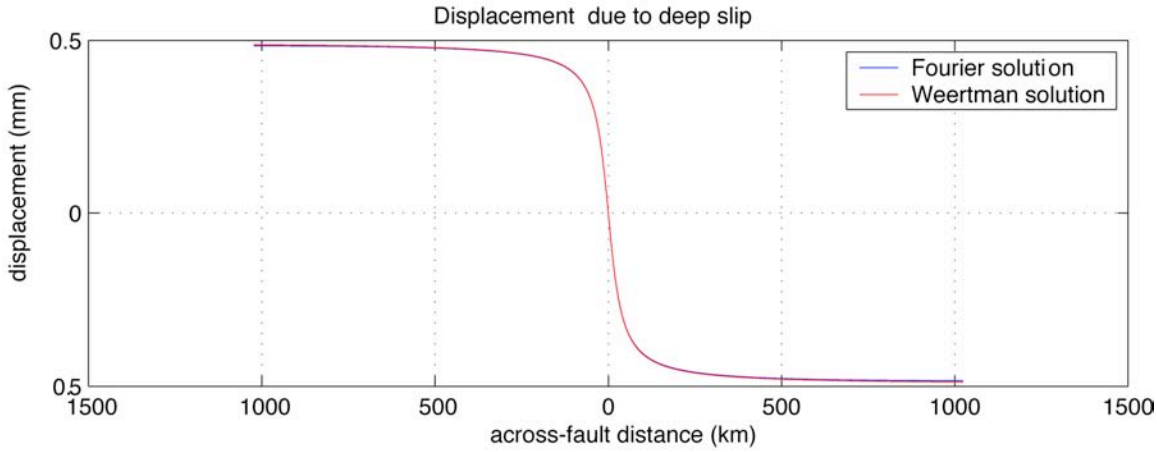

Figure 1.

The comparison between the analytic *Weertman* [1964] solution and the fault-perpendicular profile of our Fourier model provides a numerical accuracy of 10^{-3}. In order to achieve even better accuracy, the x-length of the Fourier grid must be extended to 8192 (presently 4096). A smaller dimension can be used if the fault has a finite length in the y-direction.

To test the locked-fault case (Eq. 2), we assign an upper locking depth of 1 km (d_2) and a lower locking depth of 30 km (d_1). In this model, we use the following parameters: d_1 = -30 km, d_2 = -1 km, z =0, and V_o = 1 mm. Figure 2 shows the comparison between a fault-perpendicular profile of our Fourier-derived grid results and that of the deep slip analytic solution (Eq. 2).

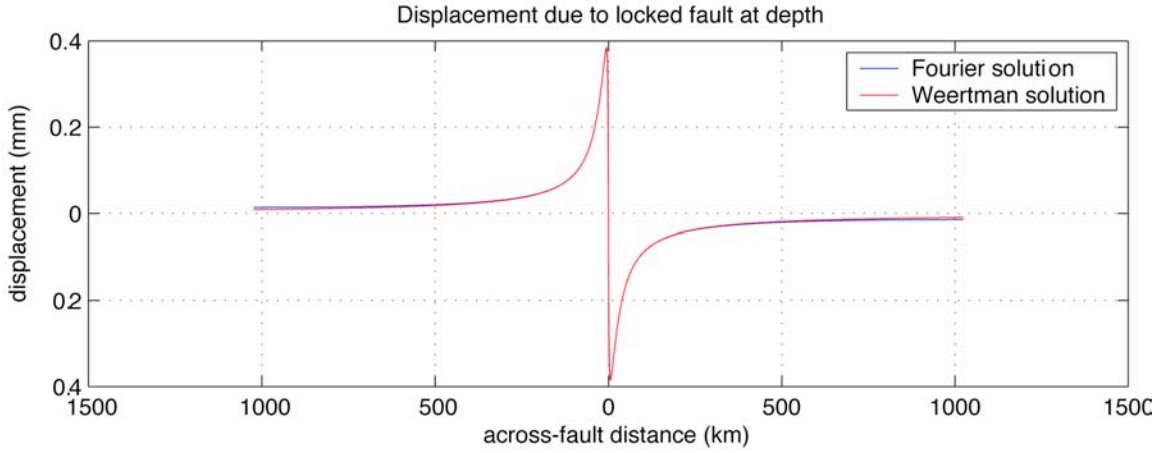

Figure 2.

Again, the comparison between the analytic *Weertman* [1964] solution and the fault-perpendicular profile of our Fourier model provides a numerical accuracy of 10^{-3}. In order to achieve even better accuracy, the *x*-length of the Fourier grid must be extended to 8192.

b) Layered elastic half-space

As a second test, we compare our Fourier-derived fault solution to the 2-D analytic solution for deformation in a *layered* elastic half-space. The surface displacement due to a 2-D fault in a layered elastic medium that is locked between depths of d_1 and d_2 [*Rybicki*, 1971] is given by:

$$V = \frac{V_o}{\pi}\left[\tan^{-1}\left(\frac{d_2}{x}\right) - \tan^{-1}\left(\frac{d_1}{x}\right) + \sum_{m=1}^{\infty}\left(\frac{\mu_1 - \mu_2}{\mu_1 + \mu_2}\right)^m \left\{\begin{array}{l}\tan^{-1}\left(\frac{d_2 - 2mH}{x}\right) - \tan^{-1}\left(\frac{d_1 - 2mH}{x}\right) \\ + \tan^{-1}\left(\frac{d_2 + 2mH}{x}\right) - \tan^{-1}\left(\frac{d_1 + 2mH}{x}\right)\end{array}\right\}\right] \quad (3)$$

where V_o= slip, d_1 = lower locking depth, d_2 = upper locking depth, H = layer thickness, μ_1 and μ_2 are layer rigidities, and m refers to the number of image terms included in the calculation (Figure 3). This solution behaves similarly to the *Weertman* [1964] solution for a homogeneous half-space, with the exception of the infinite sum term that is dependent upon the ratio of the upper and lower rigidity moduli and the plate thickness. This simple 2-D analytic solution reflects the fundamental first-order behavior of a locked fault in a layered medium and is the premise of more sophisticated layered models.

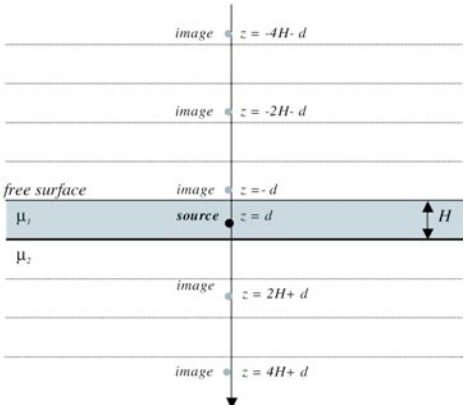

Figure 3.

Here we demonstrate three examples for our layered Fourier-derived fault solution simulating a layer of thickness H, overlying an elastic/viscoelastic half-space, depending on the ratio of rigidities, μ_1 and μ_2. In all three models, we use the following parameters: d_1= -30 km, d_2 = -1 km, H = 30 km, z = 0, and V_o = 1 mm. Our three examples will be those of:

(1) an elastic half-space ($\mu_2 = \mu_1$)
(2) an elastic layered half-space ($\mu_2 = \mu_1/3$)
(3) an elastic plate overlying a viscous half-space ($\mu_2 = 0$).

Figure 4 demonstrates the behavior of each case for the analytic solution of Eq. 3:

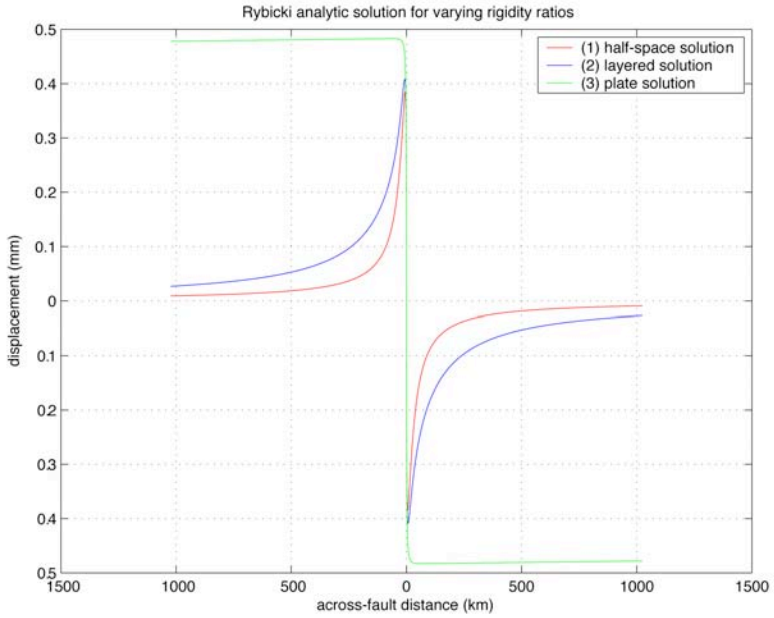

Figure 4.

(b1) Elastic half-space As a first test, we set $\mu_1 = \mu_2$ and test the case for a layered half-space of the same rigidity, better described as a homogeneous half-space. Figure 5 shows the comparison between fault-perpendicular profile of our Fourier-derived grid results and that of the analytic solution provided by *Rybicki* [1971] (Eq. 3).

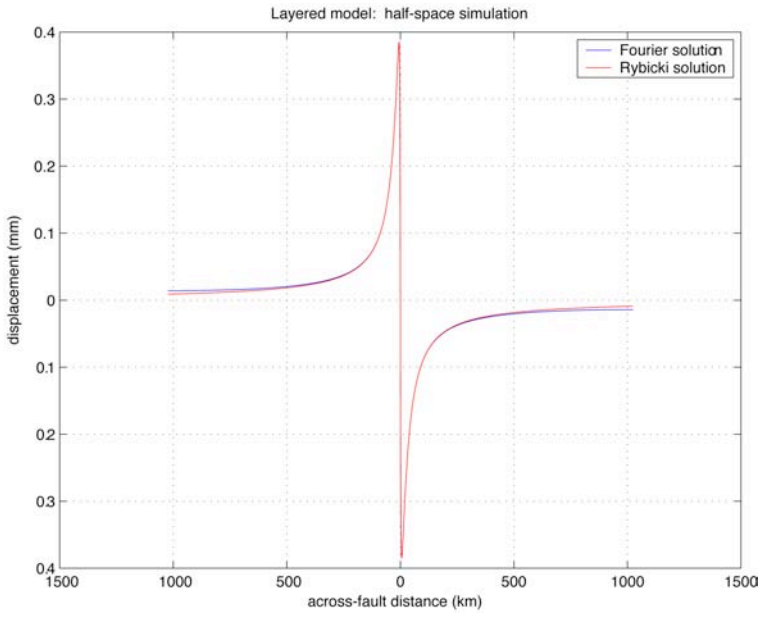

Figure 5

The comparison between the analytic solution and the fault-perpendicular profile of our Fourier model provides a numerical accuracy of 10^{-3}. This solution also matches (as it should!) the *Weertman* [1964] solution for an homogeneous half-space. This comparison is independent of the number of "*m*" terms summed in the infinite series because the rigidity ratio is always zero.

(b2) Layered half-space As a second test, we will inspect the case for a layered half-space of varying rigidities. By setting $\mu_1 = 1,\ \mu_2 = \mu_1/3$, we now require multiple terms to be summed in the infinite series because the rigidity ratio is non-zero. Convergence of the series is necessary for both the analytic solution (Eq. 3) and of our Fourier solution.

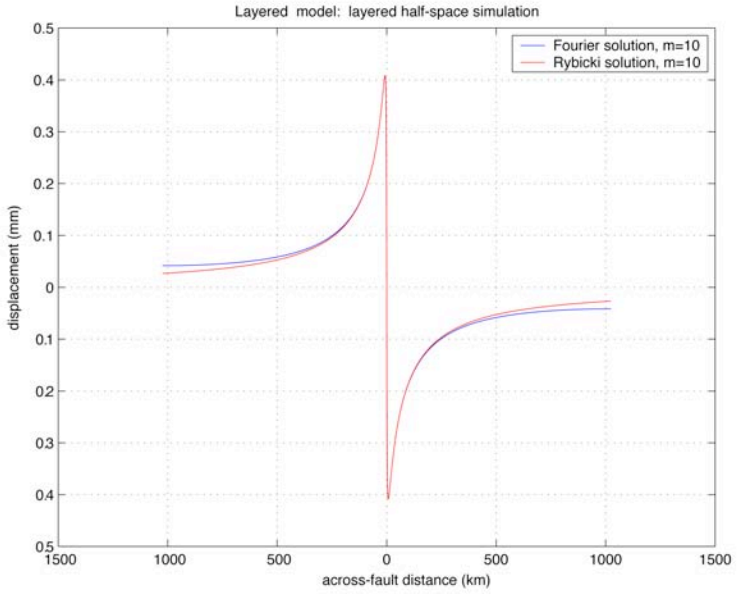

Figure 6.

Figure 6 shows the results for *m = 10* summed terms for both analytic and Fourier solutions. For the layered medium, $(\mu_1 - \mu_2 / \mu_1 + \mu_2)^m$ converges quickly. The coefficient converges to zero for terms > *m* = 10. The residual differences seen in Figure 6 in the far field are due to accuracy limitations due to grid size as mentioned before. In order to achieve even better accuracy, the *x*-length of the Fourier grid must be extended to 8192.

(b3) Elastic plate over viscous half-space As a third test, we will inspect the case for a layered half-space with the half-space rigidity set to zero, simulating an elastic plate. By setting $\mu_1 = 1,\ \mu_2 = 0$, the rigidity ratio becomes one and remains one for all summed terms. This allows for an analytic summation to be performed on the infinite series, which we invoke in our Fourier calculation. For the special case of $\mu_1 = 1,\ \mu_2 = 0$, our Fourier model will be independent of "m" terms involved in the summation, and the analytic *Rybicki* solution (Eq. 3) should converge to our Fourier solution for multiple "*m*".

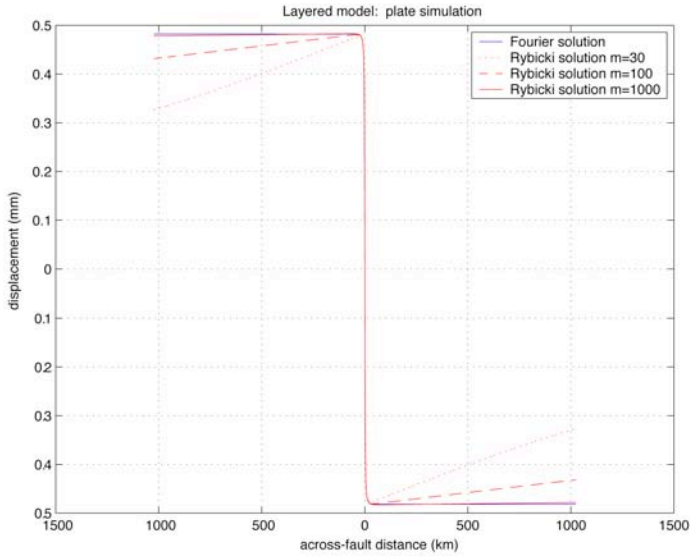

Figure 7.

From Figure 7, we again note that the analytic solution for a layered half-space slowly approaches the Fourier solution with increasing "*m*", due to the nature of the infinite series computation. For the case of an elastic plate, $(\mu_1 - \mu_2 / \mu_1 + \mu_2)^m$ fluctuates between +/-1, and thus the solution depends on the inner +/- *2mH* terms to converge. Our *fftplate.f (maxwell.f)* program makes use of the analytic form of the infinite series for a rigidity ratio of 1, and thus computes the full plate solution in one step. Alternatively, the analytic solution requires many iterations/summations in order to finally converge to the full plate solution.

c) Non-surface observation planes

Displacement can also be computed at an observation plane other than the surface ($z \neq 0$). The analytic solution for this case, taken from *Savage and Lisowski* [1993], is:

$$V(x) = \frac{V_o}{2\pi}\left[\tan^{-1}\left(\frac{x}{D-z}\right) + \tan^{-1}\left(\frac{x}{D+z}\right)\right] \qquad (4)$$

where D is the upper locking depth of an infinitely deep fault and z is the observation plane. Figure 8 shows the behavior of displacement for an infinitely-long and infinitely-deep fault locked at D = 30 km, observed at planes z = 0, 10, 30, 50, and 100 km.

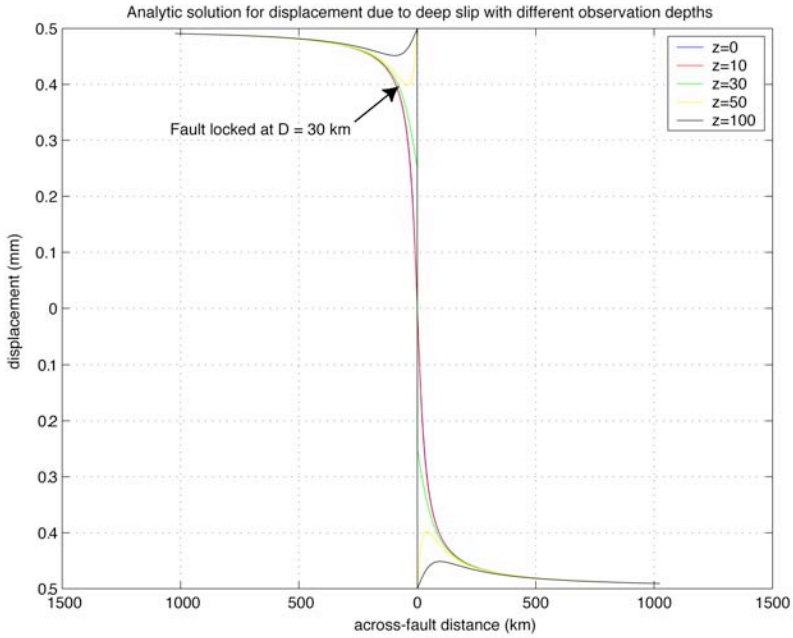

Figure 8.

Our Fourier model can also calculate both stresses and displacements within a region above or below the locked portion of the fault plane by simply segmenting the faulting-regime into two pieces and adding. Figure 9 shows the behavior of observation depth for both the analytic solution (Eq. 4) and our Fourier model:

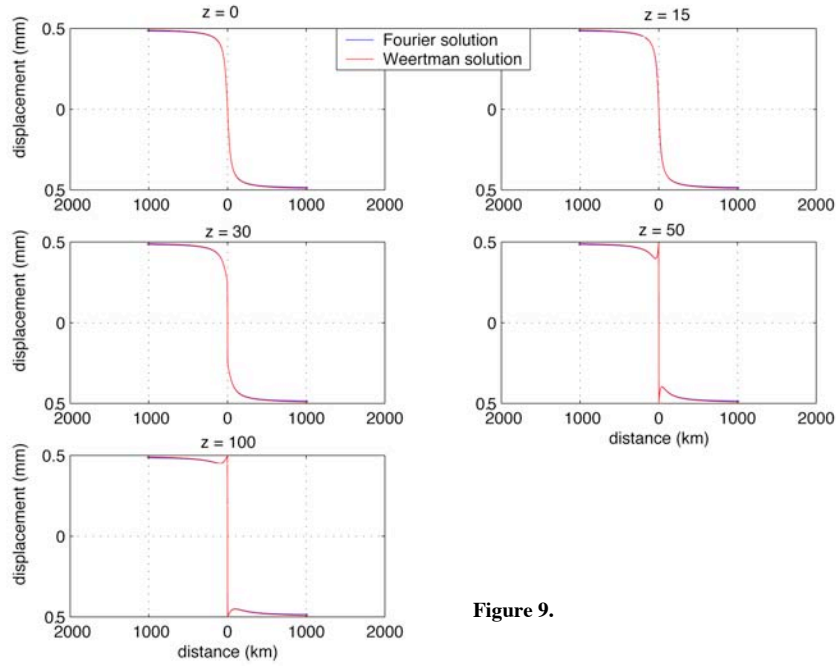

Figure 9.

d) Layered viscoelastic half-space

Our final 2-D comparison will be made with the results of *Nur and Mavko* [1974], a time-dependent version of the *Rybicki* [1971] solution that utilizes the Correspondence Principle to manipulate the rigidity of the half-space [*Savage and Prescott*, 1978; *Cohen*, 1999]. We again consider the simple case of an infinitely long vertical strike-slip fault that is imbedded in an elastic plate overlying a time-dependent Maxwell viscoelastic half-space. Within the plate, the "fault" can be thought of as two separate sections: the lower fault and the upper fault. The lower fault deforms at depths extending from the base of the locked region (d_1) to the base of the elastic plate (H). This region responds to tectonic loading during the interseismic period of the earthquake cycle. The upper portion of the fault ($d_1 - d_2$) remains locked during this time and accumulates a slip deficit, eventually leading to coseismic deformation caused by an earthquake. Postseismic displacements are caused by the relaxation of the Maxwell fluid as the elastic plate redistributes stress and the fault becomes reloaded.

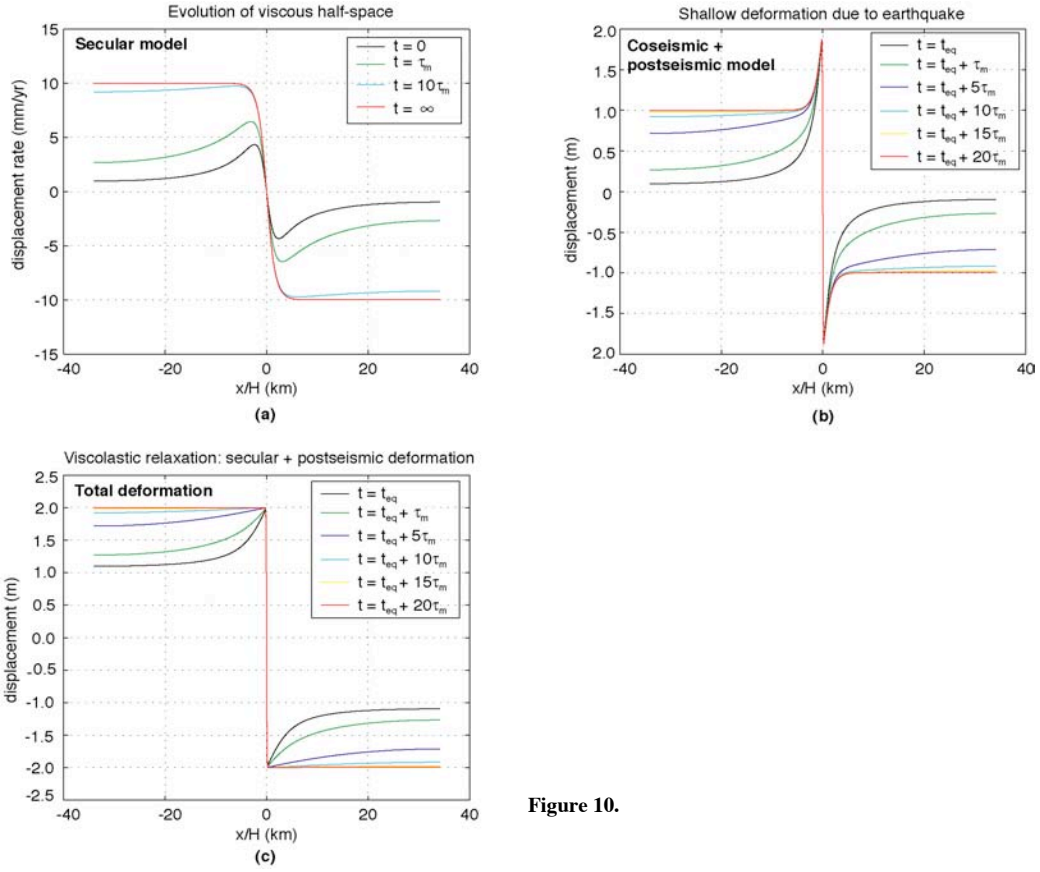

Figure 10.

Model results (Figure 10) are obtained at multiples of Maxwell time (τ_m = 24 yrs). Black ($t = 0$) and red ($t = \infty$) profile lines represent time-dependent cases reviewed by *Cohen* [1999] of the *Nur and Mavko* [1974] model. The first episode of deformation involves the geologic development of a fluid half-space (Figure 10a) where deformation occurs at depths below a locked fault that cuts halfway through a 50 km thick elastic plate. In this example, we capture the evolution of the substrate by evaluating our Fourier

model at times applicable for a homogeneous elastic half-space ($t = 0$), evolving into an elastic plate over a fluid half-space ($t = \infty$). Fault-parallel displacement profiles of Fourier model as a function of distance from the fault with respect to plate thickness, H.. A full step-function of plate velocity is achieved at times greater than $t = 100\tau_m$ or $t = \infty$, which we will henceforth refer to as the "secular model". We also demonstrate both coseismic and postseismic responses of the same locked fault that has accumulated 4 m of shallow slip (Figure 10b). Total displacement (secular model + postseismic models) produces the full 4 m of displacement (Figure 10c) at all distances from the fault. Such behavior is typical of the viscoelastic deformation problem and has been well-documented by many investigators [e.g., *Nur and Mavko*, 1974; *Rundle and Jackson*, 1977; *Savage and Prescott*, 1977; *Ward*, 1985; *Cohen*, 1999].

ii) ***Analytic Boussinesq tests***

With the exception of the 3-D elastic half-space solution [*Okada*, 1985, 1992], thus far we have only discussed 2-D model tests where the surface normal stress is zero. However, to test our model in 3-D requires testing the response of the model to vertical loads. To do this, we first compare our solution to the classic solution of *Love* [1944] for a vertical point load in a homogeneous elastic medium. We also provide a visual comparison of both homogeneous and layered half-space models with and without a gravitational restoring force. Finally, a comparison of an end-member Boussinesq model and an approximate solution to the crustal flexure problem is made [*Brotchie and Sylvester*, 1969; *Turcott and Schubert*, 1982].

a) 2-D analytic point load solution

In order to satisfy the surface boundary condition of zero shear stress, images sources are included to partially satisfy this boundary condition. But by including these extra sources, the vertical normal stress at the surface is doubled, and so the remaining task is to find a supplemental solution that cancels the normal stress without introducing additional shear stress. This problem is called the Boussinesq problem, and we address the mathematics in previous notes for the homogeneous half-space and layered half-space problems.

The basic nature of the problem is to impose a negative surface traction to match the boundary condition. This process has been likened to the 2-D analytic point load solution on an elastic half-space, discussed by *Love* [1944] in "*A Treatise on the Mathematical Theory of Elasticity*" (p. 190).

Note: z is positive down in Love's book.

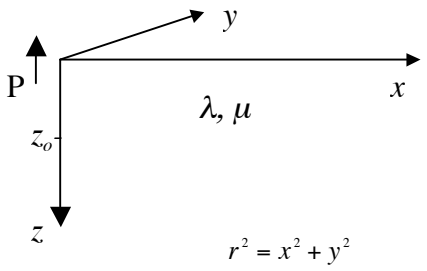

As described by *Love*, a "double force without moment", also called the center of compression (P), is applied to a single point in a cavity within a body. For simplicity, Love uses a spherical cavity and applies the single point load P at the center. The following mathematics summarized his approach:

For $z = 0$, we have the following equations describing 3-D surface displacement:

$$U(x,y) = \frac{-P}{4\pi(\lambda+\mu)}\frac{x}{r^2} \qquad V(x,y) = \frac{-P}{4\pi(\lambda+\mu)}\frac{y}{r^2} \qquad W(x,y) = \frac{P(\lambda+2\mu)}{4\pi\mu(\lambda+\mu)}\frac{1}{r}. \tag{5}$$

For $z \neq 0$, we have a slightly different set of equations:

$$U(x,y) = \frac{P}{4\pi}\left[\frac{1}{\mu}\frac{xz_0}{r^3} - \frac{1}{(\lambda+\mu)}\frac{x}{r(z+r)}\right] \qquad V(x,y) = \frac{P}{4\pi}\left[\frac{1}{\mu}\frac{yz_0}{r^3} - \frac{1}{(\lambda+\mu)}\frac{y}{r(z+r)}\right]$$
$$W(x,y) = \frac{P}{4\pi}\left[\frac{1}{\mu}\frac{z_0^2}{r^3} - \frac{(\lambda+2\mu)}{\mu(\lambda+\mu)}\frac{1}{r}\right]. \tag{6}$$

For $z \neq 0$, we can also calculate the analytic solution for vertical and horizontal stress:

$$r = \left(x^2+y^2+z^2\right)^{1/2} \qquad \frac{\partial r}{\partial x} = \frac{1}{2}\frac{1}{r}2x = \frac{x}{r}$$

$$\tau_{xx} = \lambda\left(\frac{\partial U}{\partial x}+\frac{\partial V}{\partial y}+\frac{\partial W}{\partial z}\right)+2\mu\left(\frac{\partial U}{\partial x}\right) \quad \tau_{yy} = \lambda\left(\frac{\partial U}{\partial x}+\frac{\partial V}{\partial y}+\frac{\partial W}{\partial z}\right)+2\mu\left(\frac{\partial V}{\partial y}\right)$$
$$\tau_{zz} = \lambda\left(\frac{\partial U}{\partial x}+\frac{\partial V}{\partial y}+\frac{\partial W}{\partial z}\right)+2\mu\left(\frac{\partial W}{\partial z}\right) \qquad \tau_{xy} = \mu\left(\frac{\partial U}{\partial y}+\frac{\partial V}{\partial x}\right) \tag{7}$$

For the full stress calculation, we need $\frac{\partial U}{\partial x}, \frac{\partial V}{\partial y}$, and $\frac{\partial W}{\partial z}$ (note $\frac{\partial U}{\partial y}$ and $\frac{\partial V}{\partial y} = 0$) :

$$\frac{4\pi}{P}\frac{\partial U}{\partial x} = \frac{1}{\mu}\left(zr^{-3} - 3zx^2r^{-5}\right) - \frac{1}{(\lambda+\mu)}\left[\left(rz+r^2\right)^{-1} - x\left(rz+r^2\right)^{-2}\left(\frac{zx}{r}+2x\right)\right]$$
$$\frac{4\pi}{P}\frac{\partial V}{\partial y} = \frac{1}{\mu}\left(zr^{-3} - 3zy^2r^{-5}\right) - \frac{1}{(\lambda+\mu)}\left[\left(rz+r^2\right)^{-1} - y\left(rz+r^2\right)^{-2}\left(\frac{zy}{r}+2y\right)\right] \tag{8}$$
$$\frac{4\pi}{P}\frac{\partial W}{\partial z} = \frac{1}{\mu}\left(2zr^{-3} - 3z^3r^{-5}\right) - \frac{(\lambda+2\mu)}{\mu(\lambda+\mu)}zr^{-3}$$

We will now show the results of our Fourier model for a point load on an elastic half-space. The model is run by applying a point load (F_z = 1) in the center of a grid of size 1024 x 1024 horizontal elements. The grid is then Fourier transformed, multiplied by the Boussinesq solutions, and then inverse transformed. No body forces are included for this comparison. In the analytic comparison, the point load is represented by P = 1 and the above analytic solutions are used. The observation plane is set to z = -2 to ensure short wavelength correspondence (z = -10 can be used for longer-wavelengths). The shear modulus for both models is set to $\mu = 2.6 \times 10^{10}$.

Figures 11 demonstrates, in map view, the vertical Boussinesq response (in mm) from a vertical point load applied to a homogeneous elastic half-space the displacement results of our Fourier model and the comparison with Love analytic solution.

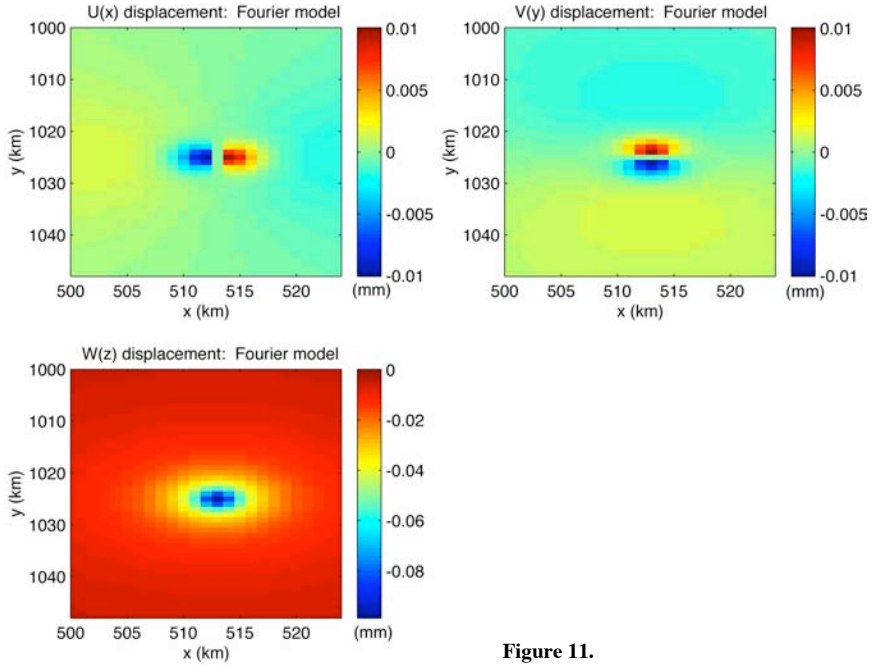

Figure 11.

Figure 12 shows both horizontal and vertical deformation from a vertical point load applied to a homogeneous elastic medium. *Love* [1944] solutions from Equation 6 are shown as blue lines (a & b) and corresponding horizontal and vertical Boussinesq solutions generated from the Fourier model are shown as red lines (a & b). Relative errors for both horizontal and vertical components are less than 1%.

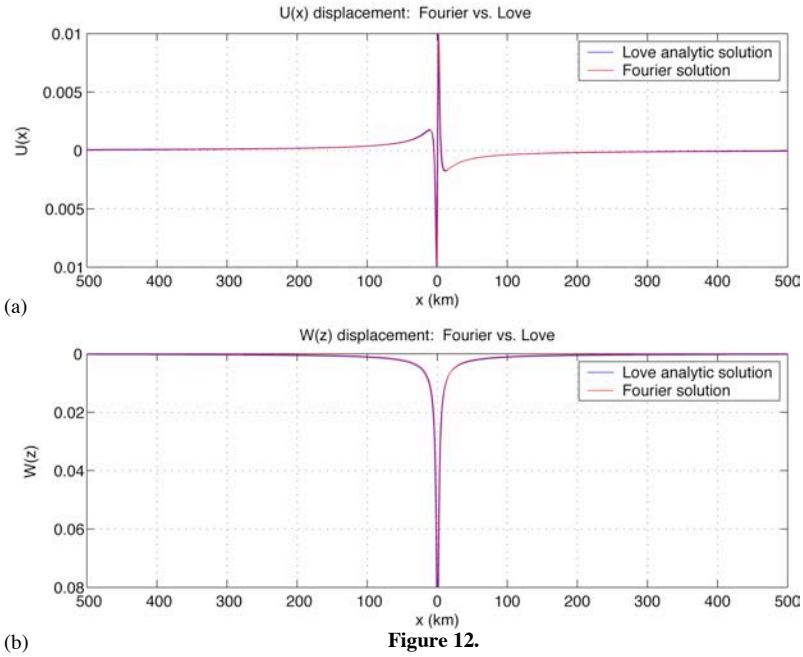

Figure 12.

Likewise, Figures 13 and 14 show the stress results of our Fourier model and the comparison with *Love* [1944] solution.

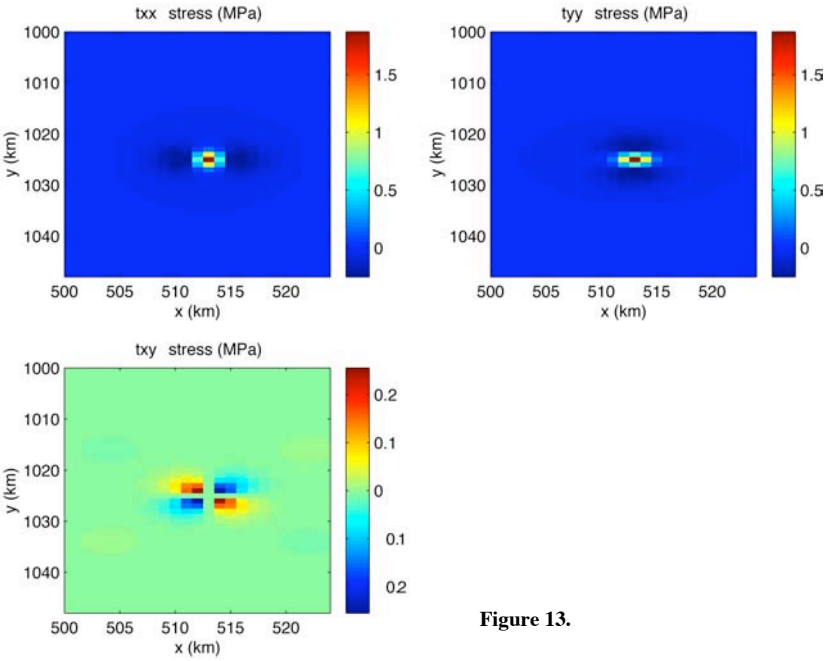

Figure 13.

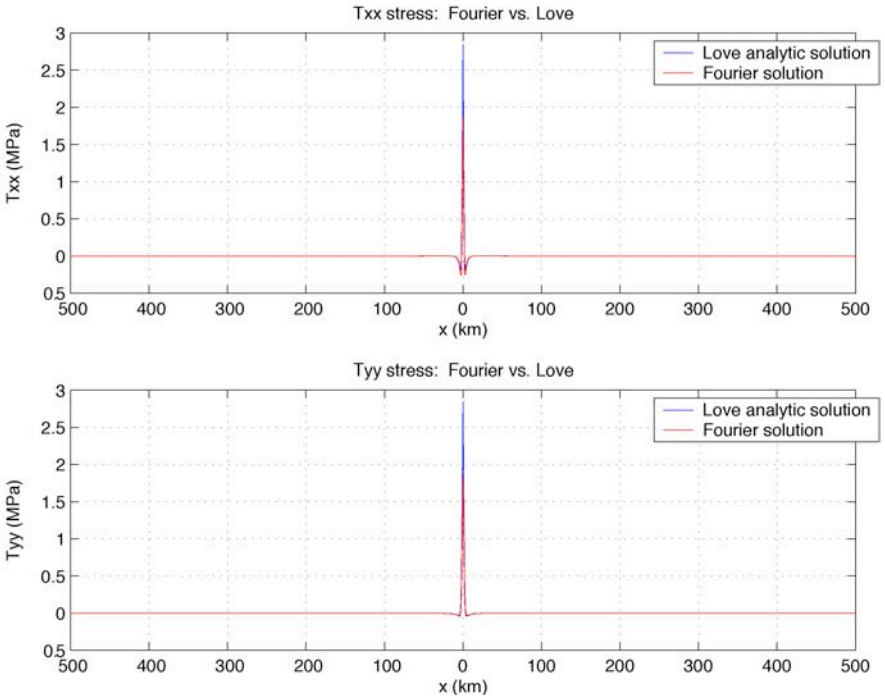

Figure 14.

b) Half-space and a plate model comparisons with gravity

We next test the accuracy and consistency of our viscoelastic Fourier model by applying a vertical point load to a variety of elastic/viscoelastic mediums As discussed in previous notes, our new Boussinesq solutions for a layered half-space can also take into the effects of gravitational support (ρg) if one wishes to do so. We have solved for the Boussinesq coefficients for the following four cases:

(1) Homogeneous half-space Boussinesq solution (no gravity)
(2) Homogeneous half-space Boussinesq solution *with* gravity
(3) Layered half-space solution (no gravity)
(4) Layered half-space solution *with* gravity

We use the coefficients obtained for these four cases to demonstrate both rheological and gravitational characteristics of vertical displacement due to a vertical point load. In the subsequent model examples we use the following parameters, F_z = 1 MPa, H = -10 km, E = 70 GPa, μ_1 = 2.6 x 10^{10} GPa, and $\eta = 10^{19}$ Pas, unless otherwise specified. For the two examples that include the effects of a layered half-space (case 3 and 4), we assume a half-space shear modulus of $\mu_2 = 0$ to simulate an elastic plate over a fluid half-space, but require the bulk modulus, κ, to remain constant:

$$\kappa = \lambda_1 + \frac{2}{3}\mu_1 \qquad \Rightarrow \qquad \lambda_2 = \kappa - \frac{2}{3}\mu_2$$

In addition, for those examples that include the gravitational contribution (case 2 and 4), ρ = 3300 kg/m^3 and g = 9.81 m/s^2.

Case (1): Homogeneous half-space Boussinesq solution (no gravity)

For this case, we assume the thickness of the elastic layer to be zero (H = 0) and compare the results of our Boussinesq solutions for a layered half-space to our previous solutions for a homogeneous half-space. The comparison provides an exact match. Figure 15a shows these results for displacement in x, y, and z (layered solution). Demonstrating similar behavior to the model of Figure 11, Figure 15a shows the z-component of deformation in a homogeneous half-space forming a negative bulls-eye region in the center of the grid.

Case (2): Homogeneous half-space Boussinesq solution *with* gravity

For this case, we assume the thickness of the elastic layer to again be zero (H = 0) and compare the results of our Boussinesq solutions for a layered half-space to those described above, this time with the addition of the gravity force balance. The comparison provides a close match to the Case (1) half-space results, but the magnitudes are slightly higher. Figure 15b shows these results for displacement in x, y, and z (layered solution). Like Figure 15a, this figure also shows the z-component of deformation forming a negative bulls-eye region in the center of the grid, although when a gravitational component is included, magnitudes become slightly larger.

Case (3): Layered half-space solution (no gravity)

For the case of an elastic plate overlying a fluid half-space, we assume the thickness of the elastic layer to be H = 10 km. A visual comparison of the results for this case (Figure 15c) shows that plate case is similar to the homogenous half-space case, but close inspection reveals that the far-field nature of the plate model retains the same sign while the half-space model reverses sign. Also note that the z-component of the plate model "blows up" to very large values. This is due to the absence of the gravitational restoring force required to balance the point load applied to the plate. While the spatial scale of this figure has been preserved for comparison with other examples, a much larger grid is required to fully capture the full bulls-eye feature. Large amplitudes are observed (over - 15 mm) because no restoring force was included to balance such deformation.

Case (4): Layered half-space solution *with* gravity

Lastly we compare the case of an elastic plate overlying a fluid half-space, this time including the effects of gravity. We assume the thickness of the elastic layer to again be H = 10 km. We compare this model to the previous (Case 3), and find a close match, but with slightly higher magnitudes for the gravity case. Also note that the z-component of the plate model with gravity now behaves as predicted, with a similar, although larger bulls-eye feature to the half-space cases. Inclusion of the gravity term (Figure 15d) eliminates the unreasonable amplitudes the previous model and produces slightly larger-scale bulls-eye feature compared to those of Figure 15a and b.

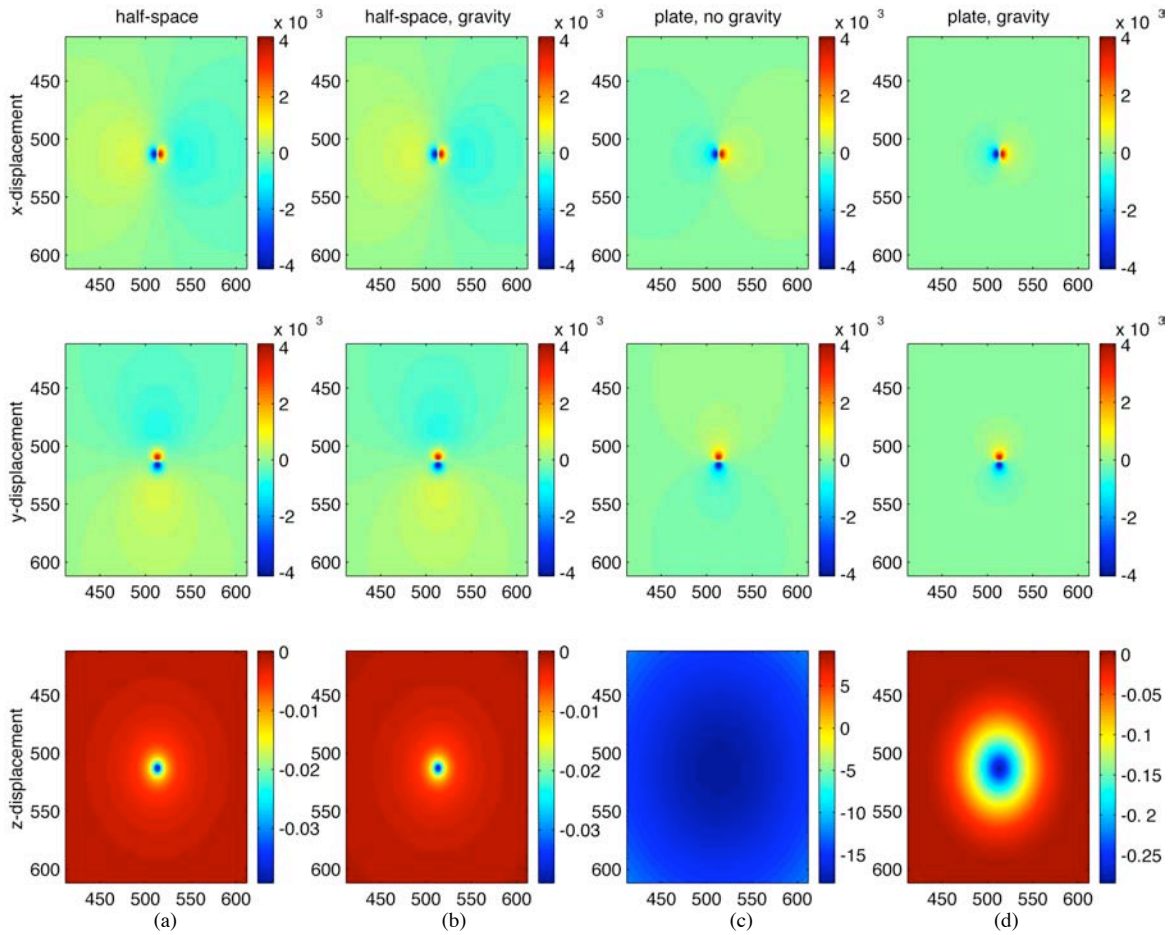

Figure 15.

c) Analytic flexure solution

The layered Boussinesq solution that includes the restoring force of gravity (Figure 5d, case 4) can be compared with an analytic solution that approximates the flexural response, *w(x)*, of a thin elastic plate due to arbitrary surface loading. The vertical force balance for flexure of a thin elastic plate floating on top of the asthenosphere [e.g., *Le Pichon*, 1973; *Sandwell*, 1982; *Turcotte and Schubert*, 2001] is described by

$$D\frac{d^4w}{dx^4} + \rho g w = P(x). \tag{12}$$

In this equation, a vertical load, *P(x),* is balanced by the flexural resistance of the plate and the gravitational restoring force, ρg. The solution for the deflection of the plate is

$$W(k) = P(k)\left[Dk^4 + \rho g\right]^{-1}, \tag{13}$$

where D is the flexural rigidity comprised of Young's modulus (E), plate thickness (H), and Poisson's ratio, υ :

$$D = \frac{EH^3}{12(1-\upsilon^2)}. \tag{14}$$

Using the same parameters as described for the previous case of the elastic plate with gravity (Figure 15d, case 4), we compare the flexure solution with the layered Boussinesq solution. Figure 16 shows, in map view, the vertical Boussinesq response (in mm) from a vertical point load applied to an elastic plate overlying a fluid half-space *with* a gravitational restoring force (Figure 16a) and the flexural response from the thin plate approximation of *Le Pichon et al.*, [1973] and *McKenzie and Bowin* [1976] (Figure 16b). The residual difference between the two models is shown in Figure 16c. The two models agree well far from the load, but due not completely agree in the center of the grid. This is due to the fact that the thin plate flexure approximation has large errors for wavelengths smaller than five times the plate thickness [*McKenzie and Bowin*, 1976], thus a mismatch is expected near the center of the load

.

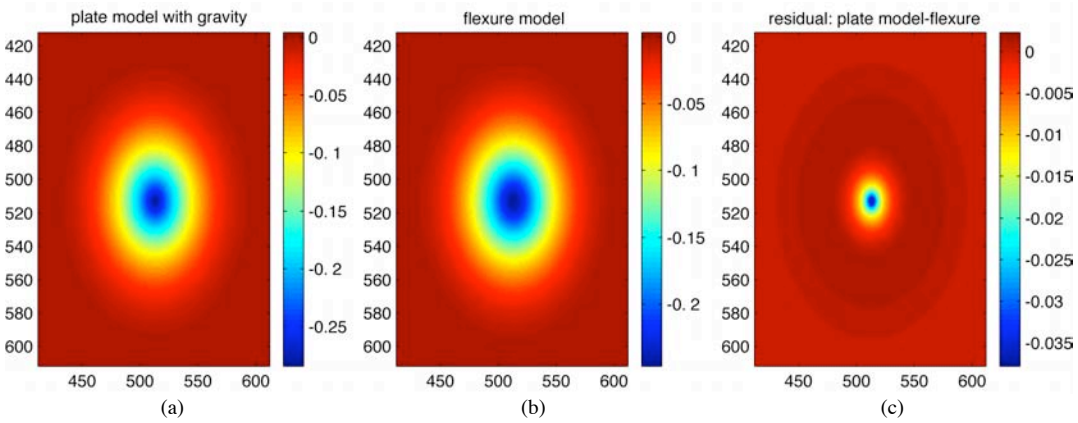

Figure 16.

This comparison of the plate model with the vertical deflection results of the flexure model shows good agreement for wavelengths greater than the plate thickness (H), although agreement is not expected for wavelengths shorter than $5H$. Profiles of these two models, along with profiles from Figures 15a and 15b better demonstrate these findings (Figure 17). Vertical profiles as a function of distance acquired for the Boussinesq results of Figures 15 and 16 for a half-space with no gravity (red, Figure 15a), a half-space with gravity (blue, Figure 15b), an elastic plate over a fluid half-space (green, Figure 16a), and the thin plate flexure approximation (black, Figure 16b).

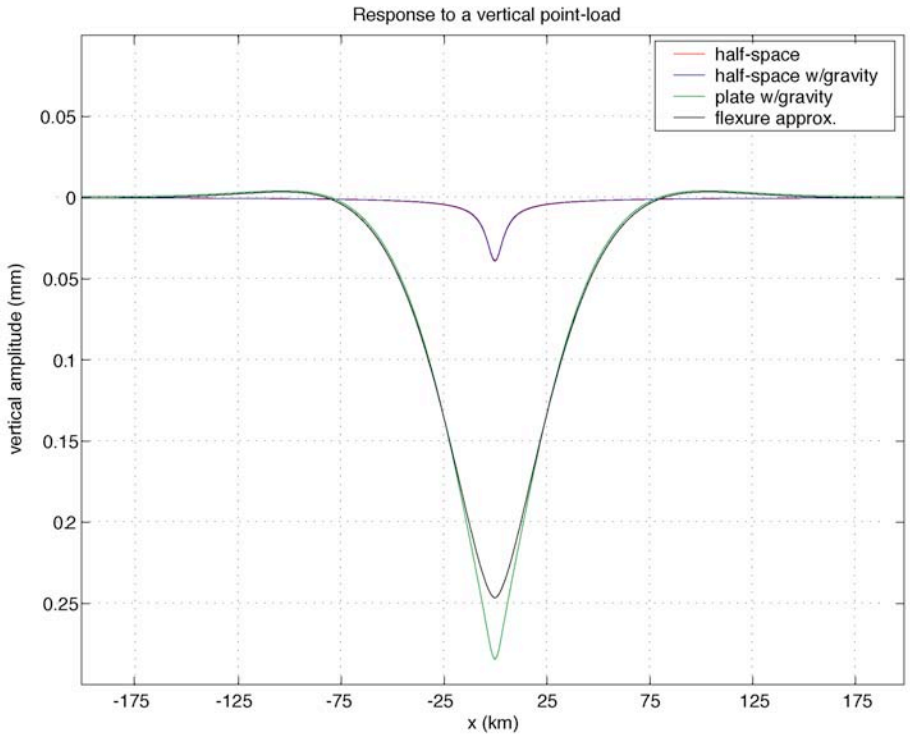

Combining the vertical results of the half-space model and the flexure solution yields a new profile with numerical accuracy of 10^{-3} when compared to the Boussinesq plate model.

d) Trench Flexure Solution

Coupling between the horizontal force and vertical response can be approximately tested in the case of trench flexure. Here we impose a moment inside of a thick elastic plate over a fluid half space. For a thin elastic plate the analytic solution to this problem is

$$w(x) = \frac{M_o \alpha^2}{2D} e^{-x/\alpha} \left[\sin(x/\alpha) - \cos(x/\alpha) \right]$$

We simulate trench flexure by applying an outward/inward stress couple as shown in the figure below.

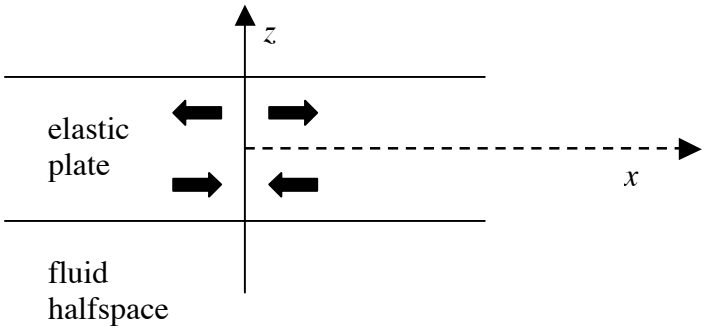

The approximate moment due to this distribution of fault-normal stress is.

$$M_o = \int_{-H/2}^{H/2} \sigma_{xx} z dz = \sigma_{xx} \frac{H^2}{4}$$

In the model we actually impose an outward/inward displacement or strain. Using the plane-stress approximation the stress and moment are.

$$\sigma_{xx} = \frac{E}{(1-\upsilon)} \varepsilon_{xx}, \qquad M_o = \frac{Eh^4}{4(1-\upsilon)} \varepsilon_{xx}$$

The comparison between the numerical model and the analytic solution is shown in the following figure.

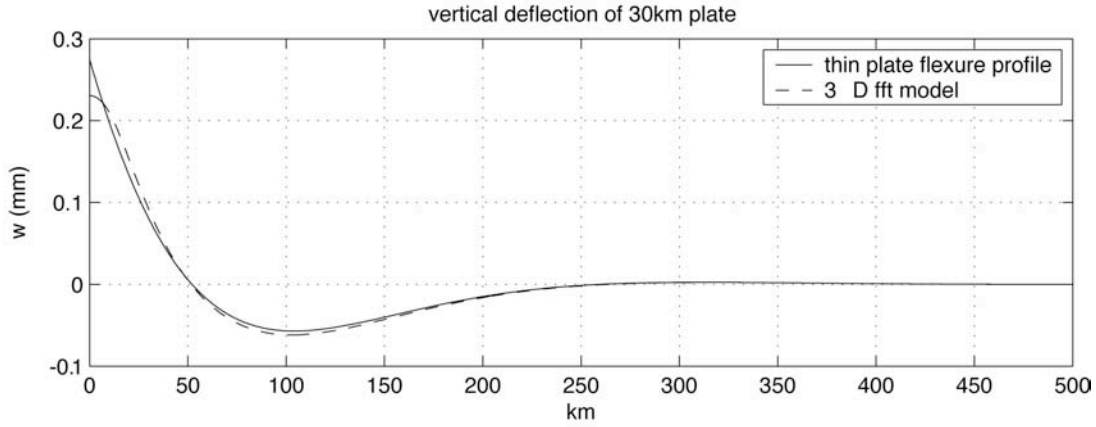

iii) ***3-D Okada model comparison***

A dislocation on a fault plane is commonly represented by body force couples. In the case of a horizontal strike-slip fault, a single-couple can be used to model deep slip simulating far-field plate boundary motion. Alternatively, a double-couple should be used to ensure local balance moment in the horizontal plane [*Burridge and Knopoff,* 1964]. The spatial variations in the force-couple are constructed by taking the derivatives of the fault function. The primary couple is parallel to the fault (*x*-direction) and corresponds to the fault-normal derivative. The secondary force couple is perpendicular to the fault (*y*-direction) and corresponds to the fault-parallel derivative.

To ensure force and moment balance, we construct a force couple by taking the derivative of a point source in the direction normal to the fault trace. In practice, the body forces due to the stress discontinuity across a fault plane are approximated by the derivative of a Gaussian function, effectively producing a model fault with a finite

thickness. For an accurate simulation, the half-width of the Gaussian must be greater than the grid size but less than the locking depth.

Here we demonstrate both single and double couple methods of our Fourier model against the results of *Okada* [1985,1992] models (double couple only) provided by *Y. Fialko*. We construct a force couple model by making the strength of the couple proportional to the long-term slip rate on a fault segment and the direction of the couple parallel to the overall plate boundary direction (not the local fault direction, if fault geometry is complex). This simulates the far-field plate tectonic force couple, which we term the "single couple model". The behavior of more shallow, co-seismic slip, though, requires a double couple to balance forces primarily in the *x*-direction. For the case of deep slip (single couple model), all forces in the *x*-direction are removed. Due to the nature of both force couples, the vector sum of all forces in the model is zero.

The steps we take in computing the vector force for both single and double couples are as follows: compute the length and orientation of the fault segment, rotate the vector into the model space, compute the Gaussian and taper effects, calculate both single and double couples. These steps are outlined further below:

Line force element source: $f(x,y) = h(x)g(y)$

h(x) = a Gaussian function with an area of 1
g(y) = a function describing the tapered ends of the fault segment

$$h(x) = \frac{1}{\sigma\sqrt{2\pi}} e^{\left(\frac{-x^2}{2\sigma^2}\right)} \qquad g(y) = \begin{cases} \frac{1}{2}\left[1 - \cos\left(\frac{\pi(y + 2\Delta y)}{4\Delta y}\right)\right] & -2\Delta y < y < 2\Delta y \\ 1 & 2\Delta y < y < L - 2\Delta y \\ \frac{1}{2}\left[1 - \cos\left(\frac{\pi(L + 2\Delta y - y)}{4\Delta y}\right)\right] & L - 2\Delta y < y < L + 2\Delta y \end{cases}$$

$$\text{primary couple}: \; f^1(x,y) = g(y)\frac{\partial h}{\partial x} \tag{15}$$

$$\text{secondary couple}: \; f^2(x,y) = \frac{\partial g}{\partial y} g(x) \tag{16}$$

$$\text{rotation into model space}: \; \begin{pmatrix} x \\ y \end{pmatrix} = \begin{pmatrix} \cos\theta & -\sin\theta \\ \sin\theta & \cos\theta \end{pmatrix} \begin{pmatrix} x' \\ y' \end{pmatrix} \tag{17}$$

In the following examples, right lateral displacement is prescribed (slip ~ -1m) and fault geometry is described by d_2 = -10.2 km, d_1 = -0.2 km, z = 0 for both models. The Fourier model assumes a completely vertical fault plane, while the *Okada* [1985,1992] model has an approximately vertical fault plane (dip = 89.99999). An 800 x 800 km size grid was used for the Fourier model computation.

a) Demonstration of single couple (deep slip) model

We first demonstrate the behavior of the single couple model by forming a single fault segment oriented in the y-direction. Following the derivative of Equation 15, Figure 18 shows the three displacement components for the single couple model.

Single Couple (Fourier model)

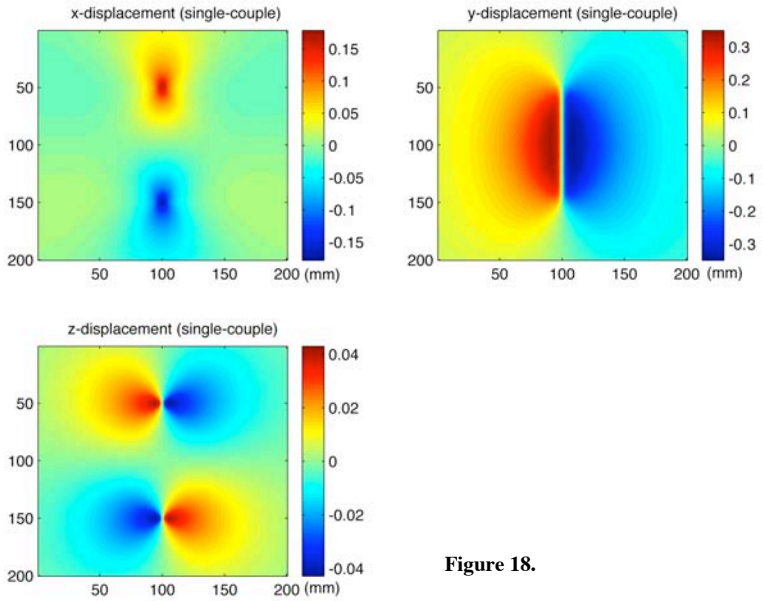

Figure 18.

b)

Demonstration of double couple (shallow slip) model

Next we demonstrate the behavior of the double couple model. Following the derivative of Equation 16, Figure 19 shows the three displacement components for the single couple model.

Double Couple (Fourier model)

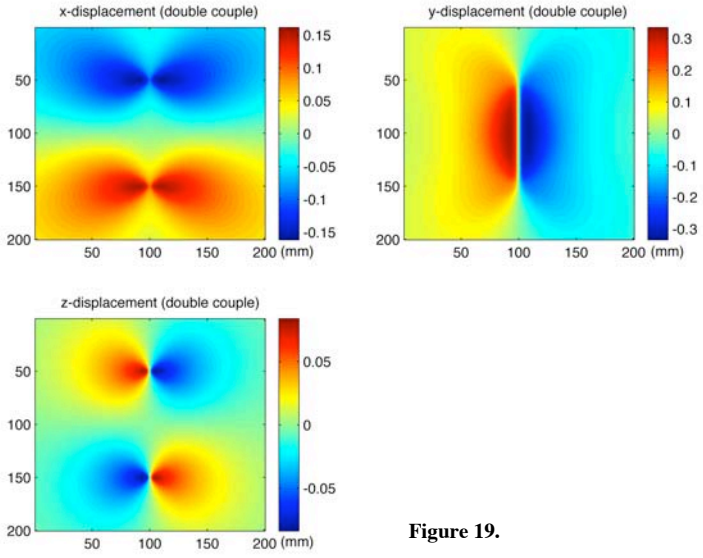

Figure 19.

Note that the differences between the double and single couples (Figure 18) lie primarily in the *x*-component. The amplitudes in the z-component are also mismatched in amplitude. Now we compare the Fourier-derived double couple model to the *Okada* [1985, 1992] model (Figure 20):

Double Couple (Okada model)

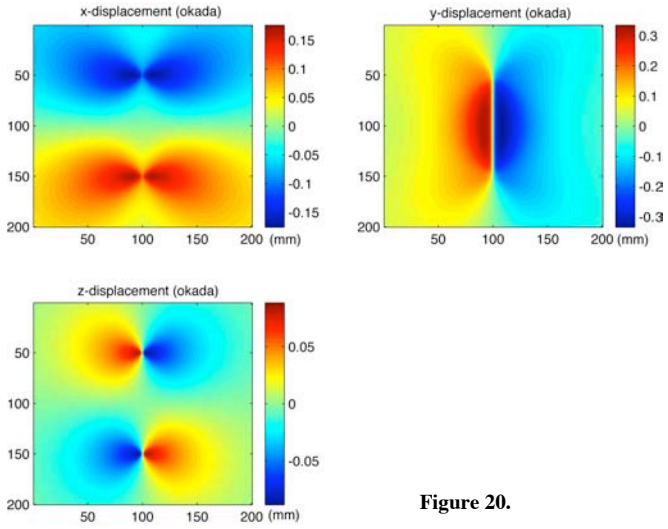

Figure 20.

Figure 21 shows across-fault profiles from y-displacement models from both Fourier and *Okada* models:

Comparison of Fourier and Okada models

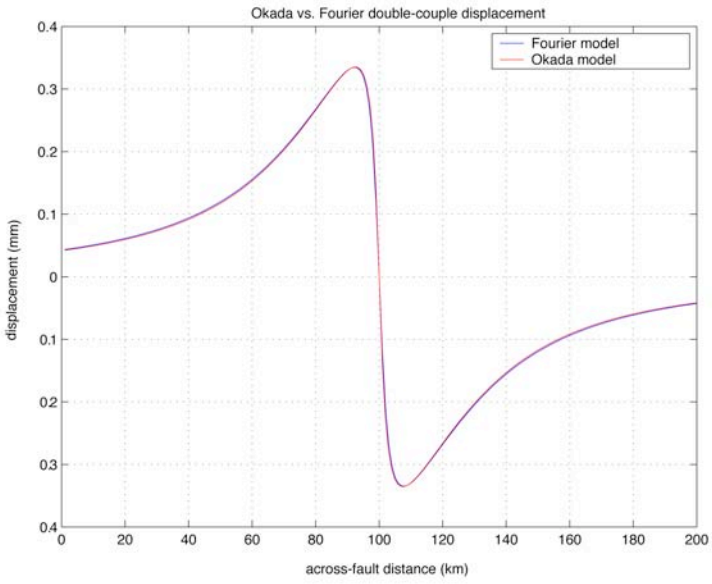

Figure 21.

Figure 22 demonstrates the numerical differences between the two models:

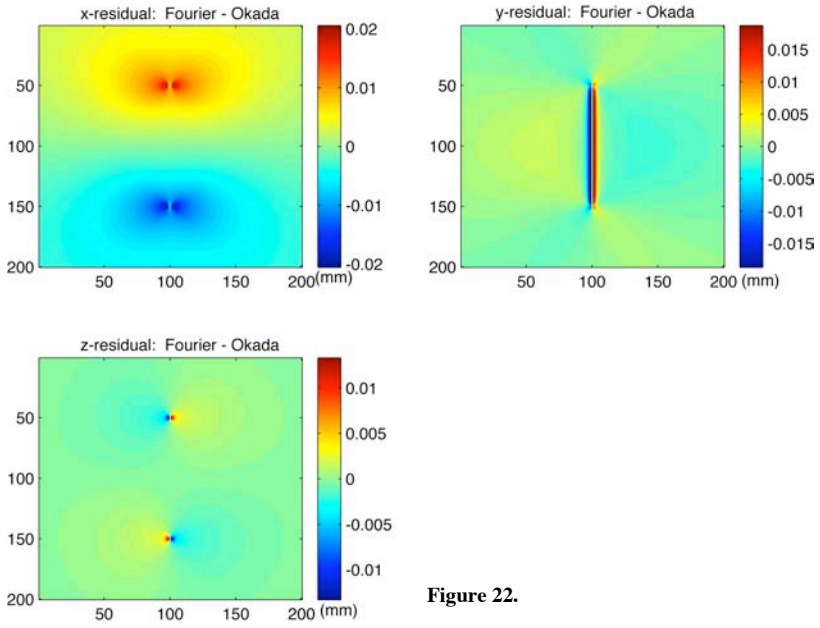

Figure 22.

Differences between the double-couple Fourier model and the *Okada* [1985, 1992] model are primarily due to the fact that we have constructed a fault of finite-width.

iv) ***Demonstration of sign convention***

The following figures (Figure 23-26) display map view results of our Fourier model for a vertical strike-slip fault of varying orientations. Right lateral displacement is prescribed (slip ~ -1m) and fault geometry is described by d_2 = -100000 km, d_1 = -10 km. Displacement is observed at a depth of z = -1 km.

a) Straight fault geometry

Case 1: N-S oriented fault

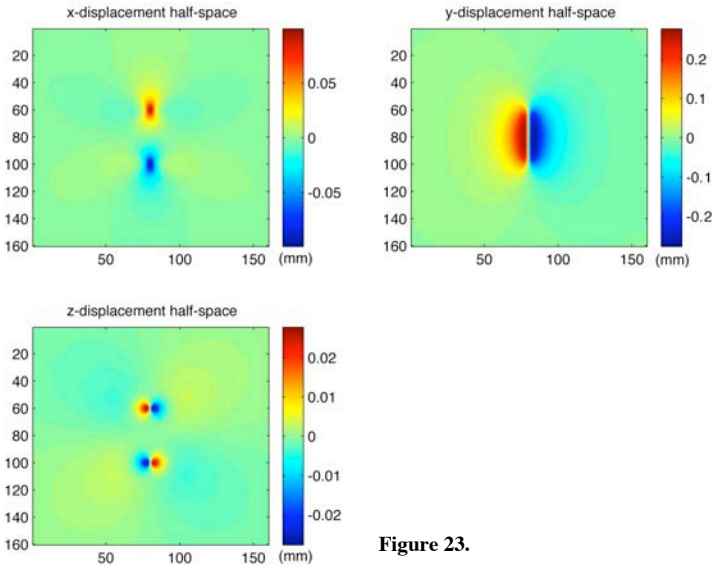

Figure 23.

Case 2: E-W oriented fault

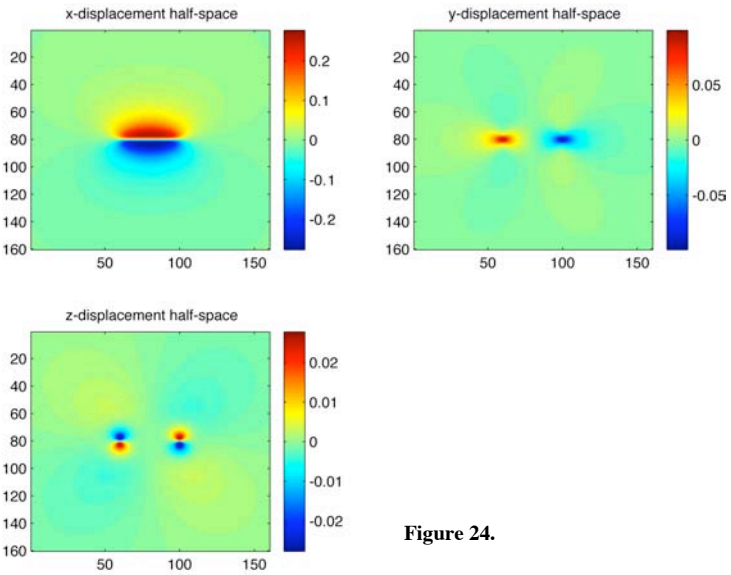

Figure 24.

b) Diagonally-oriented fault geometry

Case 3: N-S fault oriented 45° clockwise

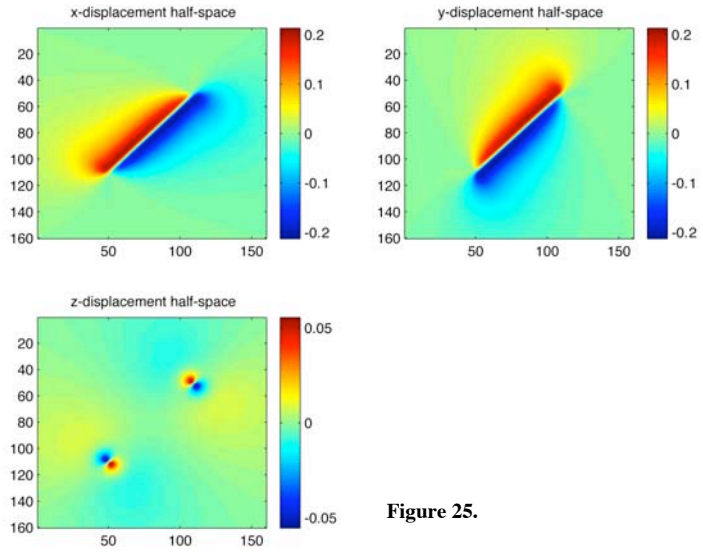

Figure 25.

Case 4: N-S fault oriented 45° counter-clockwise

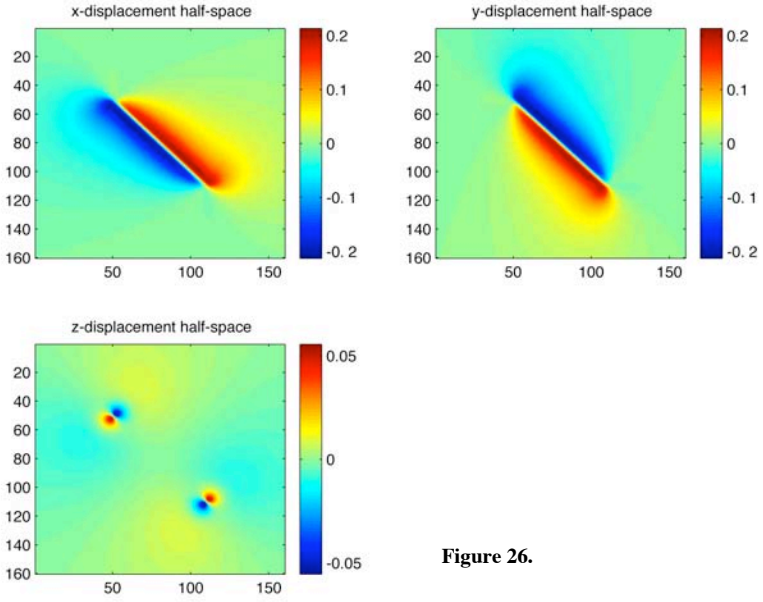

Figure 26.

v) ***Comparison of elastic and viscoelastic San Andreas model***

In order to demonstrate consistency between the original version of our Fourier model (homogeneous half-space) and the new viscoelastic Fourier model, we now compare the two for various geometries along the San Andreas Fault region.

Homogeneous half-space model: **fftfault.f** + subroutines
Layered half-space model: **maxwell.f** + subroutines

The usage of each model is as follows:

fftfault: fftfault D1 D2 Zobs ele.dat istr xd.grd yd.grd zd.grd

D1, D2 - depth to bottom and top of fault (neg)
Zobs - depth of observation plane
ele.dat - file of : x1, x2, y1, y2, F1, F2, F3
istress - (0) – disp. U, V, W, or (1) – stress Txx, Tyy, Txy
x, y, z.grd - output files of disp. or stress

maxwell: maxwell F D1 D2 Z T dble ele.dat istr U.grd V.grd W.grd

F - factor to multiply output files
D1, D2 - depth to bottom and top of fault (neg)
Z - depth of observation plane
T - time since earthquake (yr)
dble - (0-single couple, 1-double couple)
ele.dat - file of: x1,x2,y1,y2,F1,F2,F3
istress - (0)-disp. U,V,W
(1)-stress Txx,Tyy,Txy
(2)-stress Tnormal,Tshear,Tcoulomb
x,y,z.grd - output files of disp. or stress
H - plate thickness (default: H=-50km) - optional
eta - viscosity (default: eta=1.e19) - optional
pois - poissons ratio (default: pois=0.25) - optional
fd - depth factor (default: fd=1) - optional

We will make the following comparisons and checks:

(1) Displacement on an infinitely deep fault, evaluated at the surface
(2) Displacement on a shallowly-locked fault, evaluated at the surface
(3) Displacement on an intermediately-locked fault, evaluated at the surface

For all cases, the layered viscoelastic model will artificially simulate a homogenous elastic half-space by forcing the layer thickness $H \to \infty$. For this demonstration, all fault segments will be calculated at the same locking depth. All models computed with

maxwell.f have density (rho) set to zero to ensure that the layered Boussinesq subroutine defaults to that for a homogeneous elastic half-space (gravity contribution removed).

Case (1) Displacement on an infinitely deep fault, evaluated at the surface
Model parameters: D_1 = -100000 km D_2 = -1km H = -100000 km $t = \infty$

Half-space model: fftfault -100000 -1 0 all_segs_old.dat 0 xhs1.grd yhs1.grd zhs1.grd
Viscoelastic model: maxwell 1 -100000 -1 0 9999 0 all_segs.dat 0 xm1.grd ym1.grd zm1.grd -1000000 1.e19 0.25 1

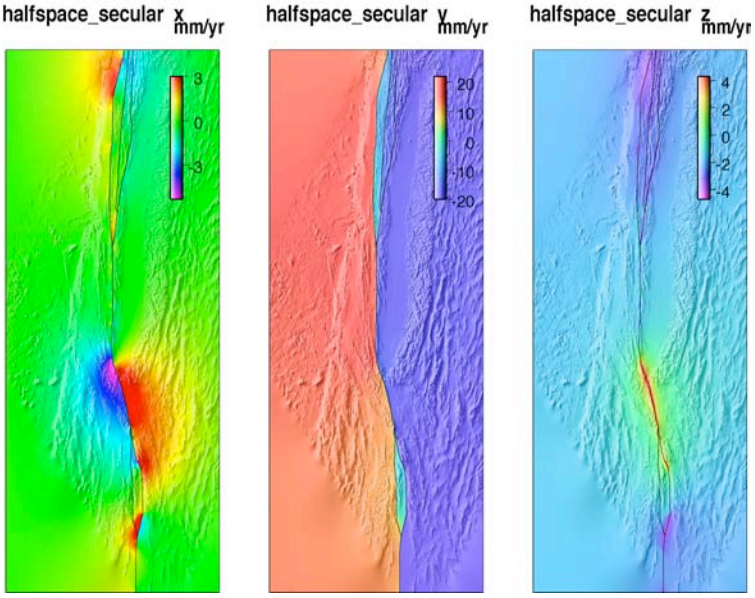

Figure 27.

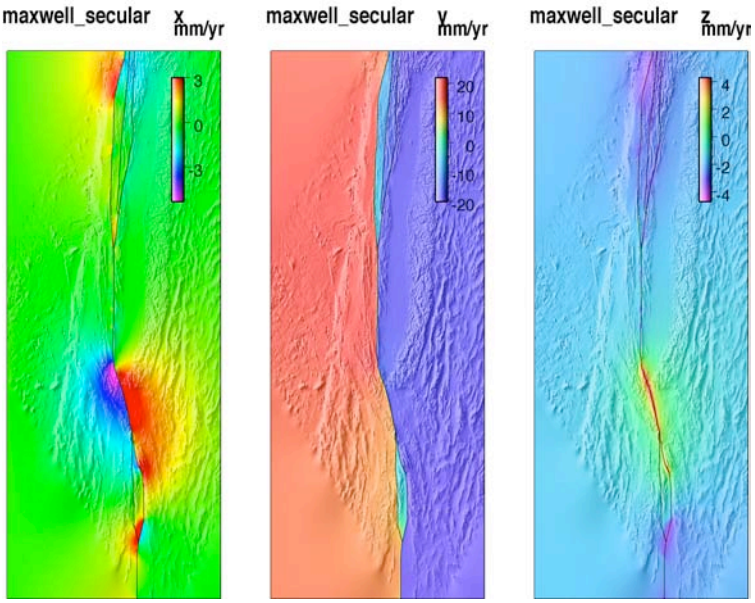

Figure 28.

Figures 27 and 28 demonstrate the 3-D results of both elastic half-space model (*fftfault.f*) and viscoelastic layered model (*maxwell.f*), respectively. The two models agree to 10^{-3} numerical accuracy for all three displacement components.

Case (2) Displacement on a shallowly-locked fault, evaluated at the surface
Model parameters: $D_1 = -10$ km $D_2 = -1$km $H = -100000$ km $t = \infty$

Half-space model: fftfault –10 –1 0 all_segs_old.dat 0 xhs2.grd yhs2.grd zhs2.grd
Viscoelastic model: maxwell 1 –10 –1 0 9999 0 all_segs.dat 0 xm2.grd ym2.grd zm2.grd
–1000000 1.e19 0.25 1

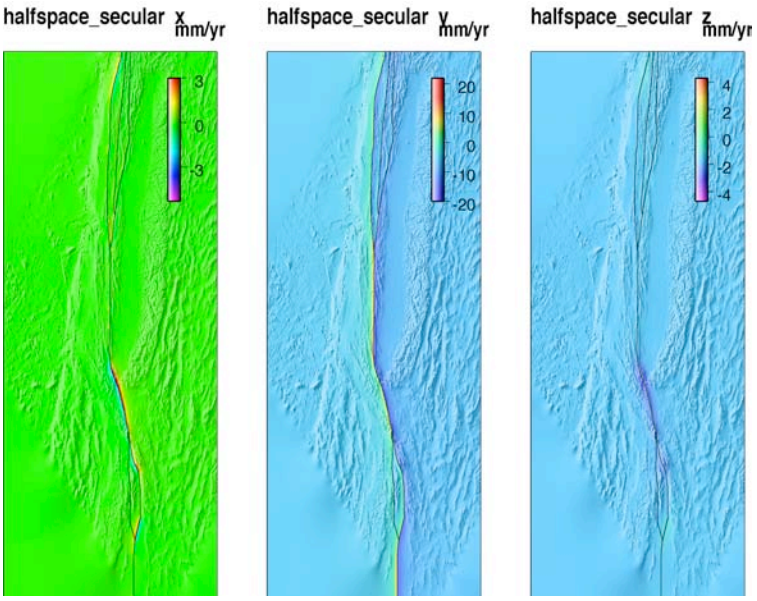

Figure 29.

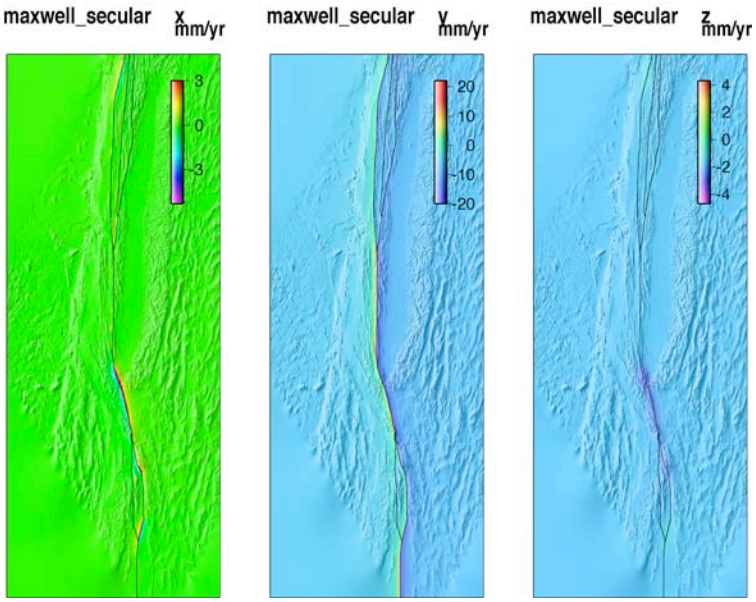

Figure 30.

Figures 29 and 30 again demonstrate the 3-D results of both elastic half-space model (*fftfault.f*) and viscoelastic layered model (*maxwell.f*), respectively, although this time for a shallow fault system. The two models again agree to 10^{-3} numerical accuracy for all three displacement components.

Case (3) Displacement on an intermediately-locked fault, evaluated at the surface
Model parameters: D_1 = -50 km D_2 = -1km H = -100000 km $t = \infty$

Half-space model: fftfault -50 –1 0 all_segs_old.dat 0 xhs3.grd yhs3.grd zhs3.grd
Viscoelastic model: maxwell 1 –50 –1 0 9999 all_segs.dat 0 xm3.grd ym3.grd zm3.grd
-100000 1.e19 .25 1

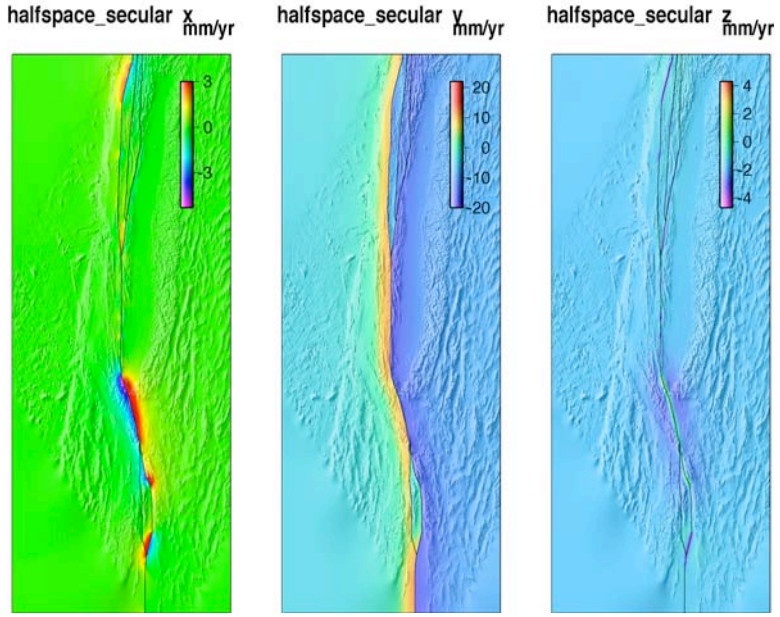

Figure 31.

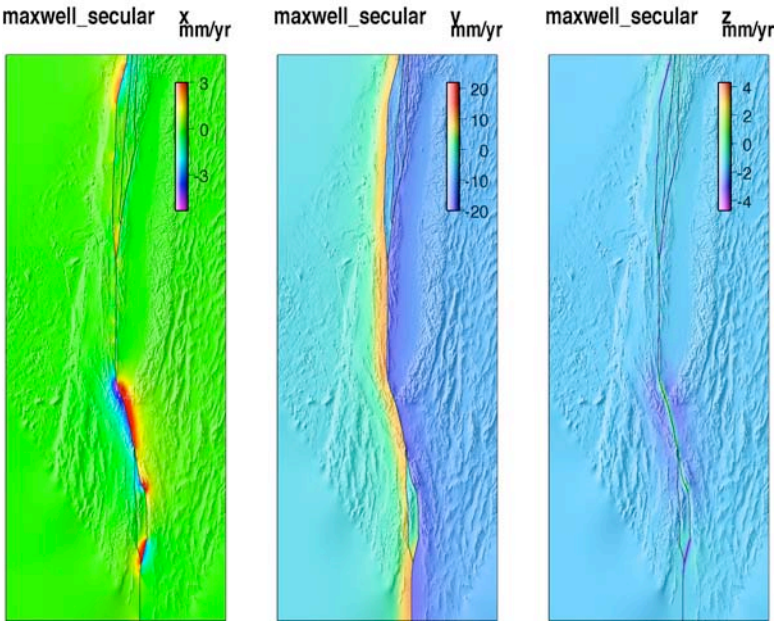

Figure 32.

Figures 31 and 32 again demonstrate the 3-D results of both elastic half-space model (*fftfault.f*) and viscoelastic layered model (*maxwell.f*), respectively, although this time for a fault system locked to 50 km. The two models again agree to 10^{-3} numerical accuracy for all three displacement components.

As a separate example, Figures 33 and 34 demonstrate the results of the *maxwell.f* model for a plate thickness of H = 50 km, with and without the restoring force of gravity (all other parameters same as above). Note how the vertical (z) component responds to a fault that cuts to the bottom of the plate. For the case without gravity (Figure 33), the vertical responds with unphysically large amplitudes, as was demonstrate in section ii by Figure 15c. When gravity is included in the calculation (Figure 34), the vertical behaves more reasonably, although with higher amplitudes than that of a homogeneous medium.

Model parameters: D_1 = -50 km D_2 = -1km H = -50 km $t = \infty$

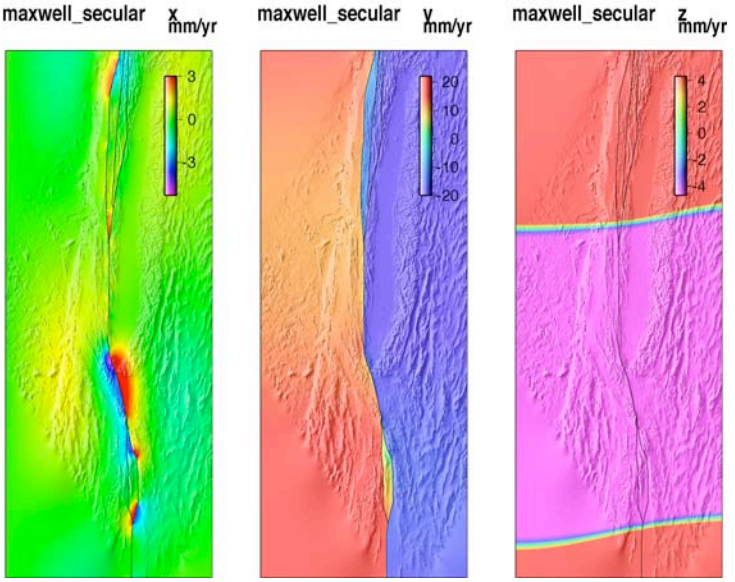

***H* = 50 km**
No gravity

Figure 33

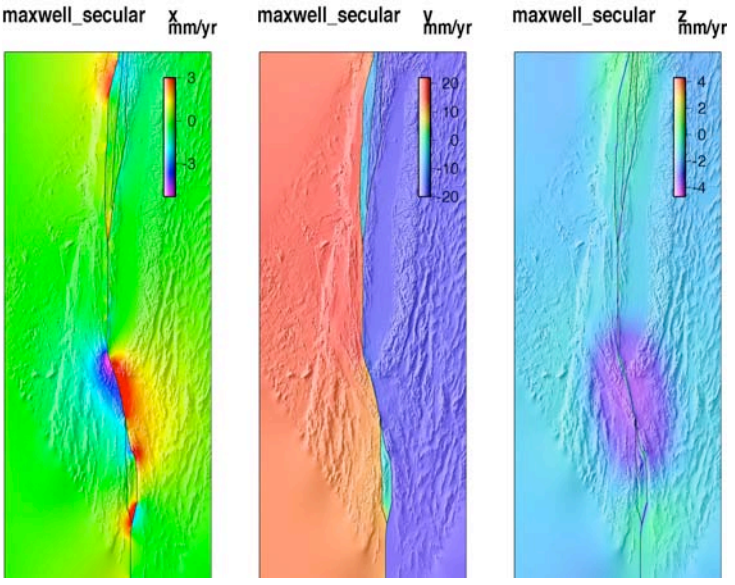

***H* = 50 km**
With gravity

Figure 34

vi) ***Example of time-dependence for viscoelastic San Andreas model***

Here we compare end-member viscoelastic models for a 50 km thick plate, where time constants $t = 0$ and $t = \infty$ are evaluated. In addition, density, p, will be incorporated back into the model to balance the vertical forces. Again, for this demonstration, all fault segments will be calculated at the same locking depth.

($t = 0$): maxwell 1 -50 -1 0 0 0 all_segs.dat 0 xm4.grd ym4.grd zm4.grd 50 1.e19 .25 1
($t = \infty$): maxwell 1 -50 -1 0 9999 0 all_segs.dat 0 xm3.grd ym3.grd zm3.grd 50 1.e19 .25

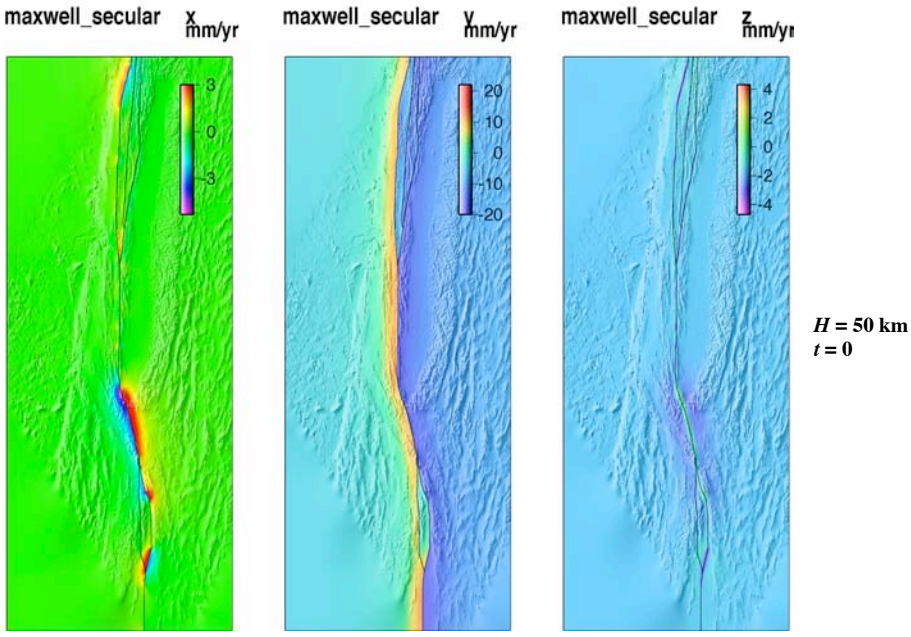

Figure 35.

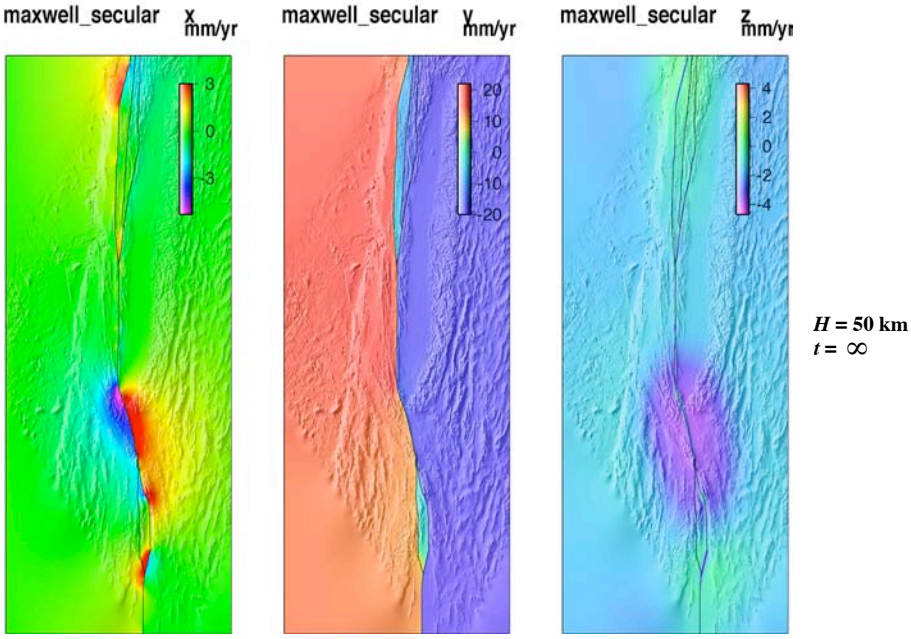

Figure 36.

Figures 35 and 36 demonstrate the 3-D results of the viscoelastic layered model (*maxwell.f*) for $t = 0$ and $t = \infty$, respectively. These results obviously differ due to the different time t parameters. Figure 35 is essentially a coseismic representation of a 50 km thick plate cut through its entirety by a 50 km deep fault, while Figure 36 represents a fully relaxed half-space that simulates the secular model.